

Spontaneous decay of quantum emitter near plasmonic nanostructure

Tigran V. Shahbazyan

Department of Physics, Jackson State University, Jackson, MS 39217 USA

We develop a theory for spontaneous decay of a quantum emitter (QE) situated near metal-dielectric structure supporting localized surface plasmons. If plasmon resonance is tuned close to the QE emission frequency, the emission is enhanced due to energy transfer from QE to localized plasmon mode followed by photon emission by plasmonic antenna. The emission rate is determined by intimate interplay between plasmon coupling to the radiation field and Ohmic losses in the metal. Here we extend our plasmon Green function approach [PRL **117**, 207401 (2016)] to include plasmon interaction with the radiation field and obtain explicit expressions for radiative decay rate and optical polarizability of a localized plasmon mode. Within this approach, we provide consistent definition of plasmon mode volume by relating it to the plasmon mode density, which characterizes plasmon field localization, and recover the standard cavity form of the Purcell factor, but now for plasmonic systems. We show that, for QE placed at "hot spot" near sharp tip of metal nanostructure, the plasmon mode volume scales with the metal volume while being very sensitive to the distance from the tip. Finally, we derive the enhancement factor for radiated power spectrum for any nanoplasmonic system and relate it to the Purcell factor for spontaneous decay rate. We illustrate our results by numerical example of a QE situated near gold nanorod tip.

I. INTRODUCTION

Rapid advances in nanoplasmonics of the past decade opened up new possibilities for extremely high energy concentration and transfer at the lengthscales well below diffraction limit [1–3]. Optical interactions between dye molecules or semiconductor quantum dots, hereafter referred to as quantum emitters (QEs), and localized plasmons in metal-dielectric structures underpin major phenomena in plasmon-enhanced spectroscopy such as surface-enhanced Raman scattering (SERS) [4], plasmon-enhanced fluorescence and luminescence [5–11], strong QE-plasmon coupling [12–23], and plasmonic laser (spaser) [24–26]. Among important issues in plasmon-enhanced spectroscopy remains consistent description of spontaneous emission by an excited dipole near plasmonic nanostructure characterized by dispersive and lossy dielectric function [27–36].

Spontaneous decay of a QE coupled to photonic or plasmonic resonator can be greatly enhanced due to additional energy transfer (ET) channel provided by cavity or plasmonic modes [37]. If the mode frequency is tuned to resonance with the QE emission frequency, the QE decay rate represents the sum of free-space decay rate γ_0^r and ET rate γ_{et} between QE and resonant mode. The rate enhancement is traditionally expressed as $\gamma = \gamma_0^r + \gamma_{et} = \gamma_0^r (1 + F_p)$, where F_p is the Purcell factor [38]. For a QE coupled to a cavity mode, the Purcell factor has the form

$$F_p = \frac{\gamma_{et}}{\gamma_0^r} = \frac{6\pi Q_m}{k^3 \mathcal{V}_m}, \quad (1)$$

where Q_m is the mode quality factor, \mathcal{V}_m is the mode volume and $k = \omega/c$ is the light wave vector (ω and c are frequency and speed of light). For photonic cavities, the mode volume at some point \mathbf{r} has the form $\mathcal{V}_{cav} = \int dV \epsilon(\mathbf{r}) |\mathbf{E}_m(\mathbf{r})|^2 / [\epsilon(\mathbf{r}) |\mathbf{E}_m(\mathbf{r})|^2]$, where $\mathbf{E}_m(\mathbf{r})$ is mode's electric field and $\epsilon(\mathbf{r})$ is (lossless) dielectric

function, and is usually interpreted as volume in which the mode would be confined at given field intensity. For photonic cavities, the mode volume is comparable to the cavity volume since, inside the cavity, the field varies weakly, while its spillover beyond the cavity is small.

Spontaneous decay of a QE coupled to *plasmonic* resonator has recently been addressed within several approaches [29–36] aiming to obtain the corresponding Purcell factor in the form (1). While the plasmon quality factor is well defined as $Q_m = \omega_m / \gamma_m$, where ω_m and γ_m are, respectively, frequency and decay rate of a plasmon mode, there has been active debate regarding how to unambiguously define plasmon mode volume if QE is located outside a metal nanostructure characterized by dispersive complex dielectric function [39–47]. For open dispersive systems, straightforward approaches based on analogy with photonic cavities do not apply, and more rigorous methods based on modal expansion of Maxwell equations' solutions are employed [48].

Here we adopt a different approach based on the observation that if the system size L is much smaller than the photon wavelength λ then, on scale $r \gg \lambda$, interaction of localized plasmons with the radiation field is analogous to that of point-like emitters with dipole moment $\mathbf{P}_m = \int dV \mathbf{P}_m$, where $\mathbf{P}_m(\mathbf{r})$ is electric polarization vector of a plasmon mode and integration takes place over the plasmonic system volume. On the other hand, on plasmonic system scale $L \ll \lambda$, spontaneous decay of a QE involves ET to the plasmon mode at a rate γ_{et} that is determined by the plasmon local density of states (LDOS) [49]. Subsequently, some part of the transferred energy is radiated away by the plasmonic antenna while the rest is dissipated in the metal. Therefore, an accurate treatment of spontaneous decay requires proper accounting, on scale $L \ll \lambda$, of the energy flow through those channels and matching it with outgoing energy flow on scale $r \gg \lambda$. As we show in this paper, this task can be accomplished by incorporating plasmon coupling to the

radiation field into plasmon LDOS in the consistent way that ensures energy flux conservation.

In the preceding paper [49], we derived the plasmon LDOS for arbitrary metal-dielectric nanostructure by including the Ohmic losses (but *not* coupling to the radiation field) and used it to describe the plasmonic enhancement of Forster ET between a donor and an acceptor. In this paper, we extend our approach to include plasmon coupling to the radiation field, and derive explicit expressions for plasmon's radiative decay rate γ_m^r and for optical polarizability of plasmonic system, which describes the system response to external field. By incorporating γ_m^r into the plasmon Green function in consistent way that ensures energy flux conservation. We then derive the Purcell factor in the form (1), where the mode volume is identified as the inverse of plasmon mode density, which characterizes plasmon field localization at the QE position. We show that, in regions near sharp tips of metal nanostructures, where plasmon fields are strongly localized (hot spots), the mode volume scales with the metal volume while their ratio is very sensitive to the QE distance from metallic tip. Finally, we derive the enhancement factor M for radiated power spectrum, which describes, e.g., plasmonic enhancement of fluorescence [5–11], and, at resonance, establish general relation $M = F_p \eta_m$, where η_m is plasmon radiation efficiency.

The paper is organized as follows. In Sec. II we revisit our derivation of the plasmon Green function [49] by using different method that makes its generalization more convenient. In Sec. III, we extend our approach to include plasmon coupling to the radiation field in a consistent way that ensures energy flux conservation, and derive explicit expressions for radiative decay rate and optical polarization of any nanoplasmonic system. In Sec. IV, we derive the plasmon LDOS, plasmon mode density, and plasmon mode volume, as well as evaluate the plasmon mode volume near sharp tip of metal nanostructure. In Sec. V, we derive the Purcel factor for spontaneous decay of a QE coupled to plasmonic resonator, and obtain explicit expression for the power spectrum enhancement factor. In Sec. VI, we illustrate our results numerically for a QE situated neat the tip of Au nanorod. A summary of our results is provided in Sec. VII, and some details of our calculations are outlined in the Appendix.

II. SPONTANEOUS DECAY AND PLASMON GREEN FUNCTION

Consider an excited QE with dipole matrix element and orientation μ and \mathbf{n} , respectively, located at some position \mathbf{r} near metal-dielectric structure described by complex dielectric function $\varepsilon(\omega, \mathbf{r}) = \varepsilon'(\omega, \mathbf{r}) + i\varepsilon''(\omega, \mathbf{r})$ and surrounded by homogeneous medium with dielectric constant ε_s . We set $\varepsilon_s = 1$ for now, but will restore it when discussing numerical examples. The full decay rate

of QE in electromagnetic environment has the form [37]

$$\gamma = \frac{8\pi\omega^2\mu^2}{c^2\hbar} \operatorname{Im} [\mathbf{n} \cdot \bar{\mathbf{G}}(\omega; \mathbf{r}, \mathbf{r}) \cdot \mathbf{n}], \quad (2)$$

where $\bar{\mathbf{G}}(\omega; \mathbf{r}, \mathbf{r}')$ is the dyadic Green dyadic for Maxwell equation satisfying $\nabla \times \nabla \times \bar{\mathbf{G}} - (\omega^2/c^2)\varepsilon \bar{\mathbf{G}} = \mathbf{I}$. For isolated QE, we have $\operatorname{Im}[\bar{\mathbf{G}}_0(\omega; \mathbf{r}, \mathbf{r})] = (\omega/6\pi c)\mathbf{I}$, yielding the free-space decay rate

$$\gamma_0^r = \frac{4\mu^2\omega^3}{3\hbar c^3}. \quad (3)$$

For systems with characteristic size below the diffraction limit, it is convenient to use rescaled Green function,

$$\bar{\mathbf{D}}(\omega; \mathbf{r}, \mathbf{r}') = \frac{4\pi\omega^2}{c^2} \bar{\mathbf{G}}(\omega; \mathbf{r}, \mathbf{r}'), \quad (4)$$

which, in the *near-field* limit, represents the sum of direct and plasmon terms, $\bar{\mathbf{D}} = \bar{\mathbf{D}}_0^{\text{nf}} + \bar{\mathbf{D}}_{\text{pl}}$ [49]. The full decay rate (2) takes the form $\gamma = \gamma_0^r + \gamma_{et}$, where

$$\gamma_{et} = \frac{2\mu^2}{\hbar} \operatorname{Im} [\mathbf{n} \cdot \bar{\mathbf{D}}_{\text{pl}}(\omega; \mathbf{r}, \mathbf{r}) \cdot \mathbf{n}] \quad (5)$$

is QE-plasmon ET rate.

A. Plasmon Green function: lossless case

For metal-dielectric system with characteristic size smaller than the radiation wavelength, the fields and frequencies of plasmon modes are determined by quasistatic Gauss law [3]

$$\nabla \cdot [\varepsilon'(\omega_m, \mathbf{r}) \nabla \Phi_m(\mathbf{r})] = 0, \quad (6)$$

where the potentials $\Phi_m(\mathbf{r})$, which satisfy standard boundary conditions across metal-dielectric interfaces, define the mode electric fields, $\mathbf{E}_m(\mathbf{r}) = -\nabla \Phi_m(\mathbf{r})$, which we chose to be real. The mode fields are orthogonal, $\int dV \mathbf{E}_m(\mathbf{r}) \cdot \mathbf{E}_n(\mathbf{r}) = \delta_{mn} \int dV \mathbf{E}_m^2(\mathbf{r})$, and regular inside the structure while falling off rapidly outside it.

In our preceding paper [49], the plasmon Green function was derived by solving the eigenvalue problem $\nabla \cdot [[\varepsilon'(\omega, \mathbf{r}) - 1] \nabla \Phi_m(\mathbf{r})] = \lambda_m(\omega) \Delta \Phi_m(\mathbf{r})$, where the plasmon frequency ω_m is determined from equation $\lambda_m(\omega_m) = -1$. In that approach, the Ohmic losses are incorporated through changes in the eigenvalues λ_m due to imaginary part of dielectric function $\varepsilon''(\omega_m, \mathbf{r})$. In this section, we provide another derivation of plasmon Green function without resorting to eigenvalue problem which allows its extension to include plasmon coupling to the radiation field in a consistent way.

The Green function $S(\omega; \mathbf{r}, \mathbf{r}')$ for quasistatic eigenvalue problem (6) satisfies equation

$$\nabla \cdot [\varepsilon(\omega, \mathbf{r}) \nabla S(\omega; \mathbf{r}, \mathbf{r}')] = 4\pi\delta(\mathbf{r} - \mathbf{r}'), \quad (7)$$

for arbitrary frequency ω . In free space ($\varepsilon = 1$), the quasistatic Green function is $S_0(\mathbf{r} - \mathbf{r}') = -1/|\mathbf{r} - \mathbf{r}'|$,

and the corresponding dyadic Green function for fields, $\bar{\mathbf{D}}_0^{\text{nf}}(\mathbf{r} - \mathbf{r}') = \nabla \nabla' S_0(\mathbf{r} - \mathbf{r}')$, coincides with the near-field limit of free-space electromagnetic Green function (4). Accordingly, after splitting S into free-space and plasmon parts, $S = S_0 + S_{\text{pl}}$, we obtain equation for S_{pl} :

$$\begin{aligned} \nabla \cdot [\varepsilon(\omega, \mathbf{r}) \nabla S_{\text{pl}}(\omega; \mathbf{r}, \mathbf{r}')] \\ = -\nabla \cdot [[\varepsilon(\omega, \mathbf{r}) - 1] \nabla S_0(\omega; \mathbf{r}, \mathbf{r}')]. \end{aligned} \quad (8)$$

Assume, for a moment, that dielectric function $\varepsilon(\omega, \mathbf{r})$ is lossless ($\varepsilon'' = 0$). For real ε , the Green function can be expanded in terms of eigenmodes of Eq. (6) as

$$S_{\text{pl}}(\omega; \mathbf{r}, \mathbf{r}') = \sum_m S_m(\omega) \Phi_m(\mathbf{r}) \Phi_m(\mathbf{r}'), \quad (9)$$

where coefficients $S_m(\omega)$ are found as follows. Applying to Eq. (8) the integral operator $\int dV \Phi_m(\mathbf{r}') \Delta'$, and using $\int dV \Phi_m(\mathbf{r}') \Delta' S_{\text{pl}}(\omega; \mathbf{r}, \mathbf{r}') = -S_m \Phi_m(\mathbf{r}) \int dV \mathbf{E}_m^2(\mathbf{r})$, we obtain

$$S_m \nabla \cdot [\varepsilon(\omega, \mathbf{r}) \nabla \Phi_m(\mathbf{r})] = 4\pi \frac{\nabla \cdot [[\varepsilon(\omega, \mathbf{r}) - 1] \nabla \Phi_m(\mathbf{r})]}{\int dV \mathbf{E}_m^2(\mathbf{r})}, \quad (10)$$

where the right hand side of Eq. (10) follows from relation $\int dV \Phi_m(\mathbf{r}') \Delta' S_0(\omega; \mathbf{r}, \mathbf{r}') = 4\pi \Phi_m(\mathbf{r})$. Then, multiplying Eq. (10) by $\Phi_m(\mathbf{r})$ and integrating over \mathbf{r} , we obtain

$$S_m(\omega) = \frac{4\pi}{\int dV \mathbf{E}_m^2(\mathbf{r})} - \frac{4\pi}{\int dV \varepsilon(\omega, \mathbf{r}) \mathbf{E}_m^2(\mathbf{r})}. \quad (11)$$

For real $\varepsilon(\omega)$, the Green function (9) with coefficients (11) is *exact* for any metal-dielectric structure with eigenmodes defined by Eq. (6). The first term in Eq. (11) ensures that $S_m = 0$ in the limit $\omega \rightarrow \infty$ (or, in free space with $\varepsilon = 1$), while the second term develops a pole, due to the Gauss law (6), as $|\omega|$ approaches ω_m .

B. Plasmon Green function: including the losses

For complex dielectric function, the plasmon pole in the Green function should move into lower half of complex plane. We assume that plasmon modes are well defined, i.e., their quality factors Q_m are sufficiently large. In the first order in $1/Q_m$, the eigenmodes Φ_m in the Green function expansion (9) are unchanged but the coefficients S_m in Eq. (11) become complex. Expanding the dielectric function near ω_m as

$$\varepsilon(\omega, \mathbf{r}) \approx \varepsilon'(\omega_m, \mathbf{r}) + \frac{\partial \varepsilon'(\omega_m, \mathbf{r})}{\partial \omega_m^2} (\omega^2 - \omega_m^2) + i\varepsilon''(\omega, \mathbf{r}), \quad (12)$$

the coefficients (11) take the form

$$S_m(\omega) = \frac{\omega_m^2}{2U_m} \frac{1}{\omega_m^2 - \omega^2 - i\omega\gamma_m(\omega)}, \quad (13)$$

where

$$U_m = \frac{1}{16\pi} \int dV \frac{\partial[\omega_m \varepsilon'(\omega_m, \mathbf{r})]}{\partial \omega_m} \mathbf{E}_m^2(\mathbf{r}) \quad (14)$$

is plasmon mode energy [50] and the rate

$$\gamma_m(\omega) = \frac{\omega_m^2}{\omega^2} \frac{W_m(\omega)}{U_m} \quad (15)$$

describes plasmon decay at frequency ω . Here $W_m(\omega)$ is power dissipated by the plasmon mode which, in the quasistatic case, is due to nonradiative (Ohmic) losses: $W_m(\omega) = W_m^{nr}(\omega)$ with [50]

$$W_m^{nr}(\omega) = \frac{\omega}{8\pi} \int dV \varepsilon''(\omega, \mathbf{r}) \mathbf{E}_m^2(\mathbf{r}). \quad (16)$$

The dyadic Green function for electric fields is given by $\bar{\mathbf{D}}_{\text{pl}}(\omega; \mathbf{r}, \mathbf{r}') = \nabla \nabla' S_{\text{pl}}(\omega; \mathbf{r}, \mathbf{r}')$, and we finally arrive at

$$\bar{\mathbf{D}}_{\text{pl}}(\omega; \mathbf{r}, \mathbf{r}') = \sum_m \frac{\omega_m^2}{2U_m} \frac{\mathbf{E}_m(\mathbf{r}) \mathbf{E}_m(\mathbf{r}')}{\omega_m^2 - \omega^2 - i\omega\gamma_m(\omega)}. \quad (17)$$

Note that the coefficients (13) are obtained by calculating the residues at the poles of function $S_m(\omega)$, given by Eq. (11). Since plasmon Green function is analytic in the complex frequency plane except isolated poles in the lower halfplane [for local dielectric function $\varepsilon(\omega, \mathbf{r})$], the expansion (17) is valid for *all* frequencies. The frequency dependence of decay rate (15) ensures that $\bar{\mathbf{D}}_{\text{pl}}(\omega; \mathbf{r}, \mathbf{r}')$ obeys the optical theorem [51]

$$\begin{aligned} \int dV \varepsilon''(\omega, \mathbf{r}) \bar{\mathbf{D}}_{\text{pl}}^*(\omega; \mathbf{r}, \mathbf{r}') \bar{\mathbf{D}}_{\text{pl}}(\omega; \mathbf{r}, \mathbf{r}'') \\ = 4\pi \text{Im} \bar{\mathbf{D}}_{\text{pl}}(\omega; \mathbf{r}', \mathbf{r}''). \end{aligned} \quad (18)$$

In the following, we assume that QE interaction with plasmonic system is dominated by a single mode and, accordingly, keep only one term in the expansion (17),

$$\bar{\mathbf{D}}_m(\omega; \mathbf{r}, \mathbf{r}') = \frac{\omega_m^2}{2U_m} \frac{\mathbf{E}_m(\mathbf{r}) \mathbf{E}_m(\mathbf{r}')}{\omega_m^2 - \omega^2 - i\omega\gamma_m(\omega)}. \quad (19)$$

In the case when ω is close to ω_m , the contribution from negative frequencies can be neglected and the plasmon Green function takes simple form [49]

$$\bar{\mathbf{D}}_m(\omega; \mathbf{r}, \mathbf{r}') = \frac{\omega_m}{4U_m} \frac{\mathbf{E}_m(\mathbf{r}) \mathbf{E}_m(\mathbf{r}')}{\omega_m - \omega - i\gamma_m/2}, \quad (20)$$

where $\gamma_m = W_m/U_m$ is the plasmon decay rate [with $W_m \equiv W_m(\omega_m)$]. Note that single-mode Green functions (19) and (20) satisfy the optical theorem (18) as well (the latter with $\omega = \omega_m$). Finally, since only metallic regions with dielectric function $\varepsilon(\omega) = \varepsilon'(\omega) + i\varepsilon''(\omega)$ contribute to U_m and W_m^{nr} , the standard plasmon decay rate due to nonradiative losses in metal is recovered,

$$\gamma_m^{nr} = \frac{W_m^{nr}}{U_m} = \frac{2\varepsilon''(\omega_m)}{\partial \varepsilon'(\omega_m)/\partial \omega_m}. \quad (21)$$

In the next section, we generalize our approach to include plasmon interaction with the radiation field.

III. INTERACTION OF PLASMON MODE WITH RADIATION FIELD

In this section, we demonstrate that the quasistatic Green function (19) can be extended to incorporate plasmon coupling to the radiation field by including plasmon's radiated power $W_m^r(\omega)$ in the decay rate (15):

$$W_m(\omega) = W_m^{nr}(\omega) + W_m^r(\omega). \quad (22)$$

Below, we derive explicit expressions for $W_m^r(\omega)$ and for the optical polarizability of plasmon mode, which characterizes plasmonic system's response to the external field.

A. Radiative decay of plasmon mode

We start with noting that radiation from a plasmonic system with characteristic size much smaller than the radiation wavelength can be treated similar to point dipole. The frequency-dependent polarization vector of plasmon mode (6) is $\mathbf{P}_m(\omega, \mathbf{r}) = \frac{1}{4\pi} [\varepsilon'(\omega, \mathbf{r}) - 1] \mathbf{E}_m(\mathbf{r})$, and its generated electric field is given by

$$\mathbf{E}_m(\omega, \mathbf{r}) = \int dV' \bar{\mathbf{D}}_0(\omega; \mathbf{r}, \mathbf{r}') \cdot \mathbf{P}_m(\omega, \mathbf{r}'), \quad (23)$$

where $\bar{\mathbf{D}}_0(\omega; \mathbf{r}, \mathbf{r}') = (4\pi\omega^2/c^2) \bar{\mathbf{G}}_0(\omega; \mathbf{r}, \mathbf{r}')$ is the free-space dyadic Green function. The power dissipated by plasmon mode through radiation is given by [37]

$$\begin{aligned} W_m^r(\omega) &= \frac{\omega}{2} \text{Im} \int dV \mathbf{E}_m(\omega, \mathbf{r}) \cdot \mathbf{P}_m(\omega, \mathbf{r}) \\ &= \frac{\omega}{2} \text{Im} \int dV \int dV' \mathbf{P}_m(\omega, \mathbf{r}) \cdot \bar{\mathbf{D}}_0(\omega; \mathbf{r}, \mathbf{r}') \cdot \mathbf{P}_m(\omega, \mathbf{r}'), \end{aligned} \quad (24)$$

where integration takes place over plasmonic system volume. Replacing the free-space Green function by its near-field limit, $\text{Im}\bar{\mathbf{D}}_0(\omega; \mathbf{r}, \mathbf{r}') = (2\omega^3/3c^3) \mathbf{I}$, we obtain

$$W_m^r(\omega) = \frac{\omega^4}{3c^3} \mathcal{P}_m^2(\omega), \quad (25)$$

where

$$\mathcal{P}_m(\omega) = \frac{1}{4\pi} \int dV [\varepsilon'(\omega, \mathbf{r}) - 1] \mathbf{E}_m(\mathbf{r}) \quad (26)$$

is plasmon's dipole moment. Same result is obtained by integrating Poynting's vector $S = (c/8\pi) |\mathbf{E}_m(\omega, \mathbf{r})|^2$ over remote surface enclosing the system. Note that plasmon's radiated power (25) coincides with that of a point dipole $\mathcal{P}_m(\omega)$ [37]. By including the radiated power (25) into full dissipated power (22), the radiative decay channel is incorporated, via decay rate (15), within the plasmon Green function (19) in a way that ensures energy flux conservation (see below).

Near plasmon resonance, the plasmon decay rate in the Green function (20) takes the form $\gamma_m = \gamma_m^{nr} + \gamma_m^r$, where

the plasmon radiation rate is obtained by normalizing radiated power with mode energy,

$$\gamma_m^r = \frac{W_m^r}{U_m} = \frac{\omega_m^4}{3c^3} \frac{\mathcal{P}_m^2}{U_m}, \quad (27)$$

which, upon using Eqs. (14) and (26), takes the form

$$\gamma_m^r = \frac{\omega_m^4}{3\pi c^3} \frac{[\int dV (\varepsilon' - 1) \mathbf{E}_m(\mathbf{r})]^2}{\int dV (\partial \omega_m \varepsilon' / \partial \omega_m) \mathbf{E}_m^2(\mathbf{r})}, \quad (28)$$

where we denoted $W_m^r \equiv W_m^r(\omega_m)$, $\mathcal{P}_m \equiv \mathcal{P}_m(\omega_m)$ and, under the integral, $\varepsilon \equiv \varepsilon(\omega_m, \mathbf{r})$. Correspondingly, the plasmon radiation efficiency η_m has the form

$$\eta_m = \frac{\gamma_m^r}{\gamma_m^{nr}} = \frac{\zeta_m}{1 + \zeta_m}, \quad (29)$$

where the parameter

$$\zeta_m = \frac{\gamma_m^r}{\gamma_m^{nr}} = \frac{\omega_m^3}{6\pi c^3} \frac{[\int dV (\varepsilon' - 1) \mathbf{E}_m(\mathbf{r})]^2}{\int dV \varepsilon'' \mathbf{E}_m^2(\mathbf{r})}, \quad (30)$$

characterizes radiative decay rate relative to nonradiative one. For small plasmonic systems, γ_m^{nr} should also include the Landau damping rate [52]. Note that, in contrast to field-independent nonradiative decay rate (21), the radiative decay rate (28) *does* depend on plasmon field's distribution in the system albeit not on its overall magnitude. Such "nonanalytic" field dependence of γ_m^r , which is present in the Landau damping rate as well [52], reflects the fact that, in contrast to point dipole, local fields can noticeably vary on the plasmonic system scale.

B. Optical polarizability of a plasmonic system in the external field and energy flux conservation

Here we show that the plasmon Green function that incorporates Ohmic and radiation losses ensures the standard relation between plasmon absorption, scattering and extinction crosssections, $\sigma_{abs} + \sigma_{sc} = \sigma_{ext}$, and derive the optical polarizability of plasmon mode which describes plasmonic system's resonant response to the external field. For resonant mode, we use the single-mode plasmon Green function (19) and, accordingly, omit nonresonant contributions.

1. Energy flux conservation

Consider response of plasmonic system to incident monochromatic field $\mathbf{E}_i e^{-i\omega t}$ that is uniform on the system scale. The electric field scattered off the plasmonic structure has the form

$$\mathbf{E}_{sc}(\omega, \mathbf{r}) = \int dV' \chi(\omega, \mathbf{r}') \bar{\mathbf{D}}(\omega; \mathbf{r}, \mathbf{r}') \cdot \mathbf{E}_i, \quad (31)$$

where $\chi(\omega, \mathbf{r}) = [\varepsilon(\omega, \mathbf{r}) - 1]/4\pi$ is plasmonic system susceptibility that restricts the integration within plasmonic system volume and $\bar{\mathbf{D}}(\omega; \mathbf{r}, \mathbf{r}')$ is the dyadic Green function (4). The power absorbed by plasmonic structure is

$$W_{\text{abs}}(\omega) = \frac{\omega}{8\pi} \int dV \varepsilon''(\omega, \mathbf{r}) |\mathbf{E}_{\text{sc}}(\omega, \mathbf{r})|^2. \quad (32)$$

Inside the plasmonic structure, we replace $\bar{\mathbf{D}}(\omega; \mathbf{r}, \mathbf{r}')$ in Eq. (31) with the plasmon Green function $\bar{\mathbf{D}}_m(\omega; \mathbf{r}, \mathbf{r}')$, given by Eq. (19), and after some algebra we obtain

$$W_{\text{abs}}(\omega) = W_m^{nr}(\omega) |S_m(\omega)|^2 [\mathbf{P}_m(\omega) \cdot \mathbf{E}_i]^2, \quad (33)$$

where the functions $S_m(\omega)$, $W_m^{nr}(\omega)$, and $\mathbf{P}_m(\omega)$ are given by Eqs. (13), (16) and (26), respectively. Normalizing $W_{\text{abs}}(\omega)$ by the incident energy flux $S_i = (c/8\pi)\mathbf{E}_i^2$, we obtain resonant absorption crosssection

$$\sigma_{\text{abs}}(\omega) = \frac{4\pi\omega}{c} \frac{\omega_m^2}{2U_m} \frac{\omega\gamma_m^{nr}(\omega) [\mathbf{e} \cdot \mathbf{P}_m(\omega)]^2}{(\omega_m^2 - \omega^2)^2 + \omega^2\gamma_m^2(\omega)}, \quad (34)$$

where plasmon decay rates $\gamma_m(\omega)$ and $\gamma_m^{nr}(\omega)$ are given by Eq. (15) with $W_m(\omega)$ and $W_m^{nr}(\omega)$, respectively, and \mathbf{e} is incident field polarization.

To obtain scattering crosssection, we extract the far field contribution from Eq. (31) with help of the Dyson equation for dyadic Green function,

$$\begin{aligned} \bar{\mathbf{D}}(\omega; \mathbf{r}, \mathbf{r}') &= \bar{\mathbf{D}}_0(\omega; \mathbf{r}, \mathbf{r}') \\ &+ \int dV_1 \chi(\omega, \mathbf{r}_1) \bar{\mathbf{D}}_0(\omega; \mathbf{r}, \mathbf{r}_1) \cdot \bar{\mathbf{D}}(\omega; \mathbf{r}_1, \mathbf{r}'). \end{aligned} \quad (35)$$

Keeping the resonance term and replacing $\bar{\mathbf{D}}(\omega; \mathbf{r}_1, \mathbf{r}')$ by the plasmon Green function (19), we integrate the energy flux $S = (c/8\pi) |\mathbf{E}_{\text{sc}}(\omega, \mathbf{r})|^2$ over remote surface enclosing the plasmonic system to obtain

$$W_{\text{sc}}(\omega) = W_m^r(\omega) |S_m(\omega)|^2 [\mathbf{P}_m(\omega) \cdot \mathbf{E}_i]^2, \quad (36)$$

where $W_m^r(\omega)$ is given by Eq. (25). Normalizing $W_{\text{sc}}(\omega)$ by incident flux, we get resonant scattering crosssection

$$\sigma_{\text{sc}}(\omega) = \frac{4\pi\omega}{c} \frac{\omega_m^2}{2U_m} \frac{\omega\gamma_m^r(\omega) [\mathbf{e} \cdot \mathbf{P}_m(\omega)]^2}{(\omega_m^2 - \omega^2)^2 + \omega^2\gamma_m^2(\omega)}, \quad (37)$$

where plasmon radiative decay rate $\gamma_m^r(\omega)$ is given by Eq. (15). Adding $\sigma_{\text{sc}}(\omega)$ and $\sigma_{\text{abs}}(\omega)$, we obtain resonant extinction crosssesction as

$$\sigma_{\text{ext}}(\omega) = \frac{4\pi\omega}{c} \frac{\omega_m^2}{2U_m} \frac{\omega\gamma_m(\omega) [\mathbf{e} \cdot \mathbf{P}_m(\omega)]^2}{(\omega_m^2 - \omega^2)^2 + \omega^2\gamma_m^2(\omega)}, \quad (38)$$

where we used the relation $\gamma_m(\omega) = \gamma_m^{nr}(\omega) + \gamma_m^r(\omega)$, which, here, is equivalent to the energy flux conservation:

$$\sigma_{\text{abs}}(\omega) = \frac{\gamma_m^{nr}(\omega)}{\gamma_m(\omega)} \sigma_{\text{ext}}(\omega), \quad \sigma_{\text{sc}}(\omega) = \frac{\gamma_m^r(\omega)}{\gamma_m(\omega)} \sigma_{\text{ext}}(\omega). \quad (39)$$

2. Optical polarizability of plasmon mode

We can now obtain optical response functions for plasmonic nanostructures using the standard relation

$$\sigma_{\text{ext}}(\omega) = \frac{4\pi\omega}{c} \text{Im}[\mathbf{e} \cdot \bar{\alpha}(\omega) \cdot \mathbf{e}], \quad (40)$$

where $\bar{\alpha}_m(\omega)$ is *plasmon polarizability* dyadic, which characterizes plasmonic system's response to the external field polarized along \mathbf{e} . From Eq. (38), we obtain

$$\bar{\alpha}_m(\omega) = \frac{\omega_m^2}{2U_m} \frac{\mathbf{P}_m(\omega) \mathbf{P}_m(\omega)}{\omega_m^2 - \omega^2 - i\omega\gamma_m(\omega)}. \quad (41)$$

The polarizability (41) can be split into scattering and absorbing parts (suppressing ω -dependence)

$$\bar{\alpha}_m'' = \frac{\gamma_m^r}{\gamma_m} \bar{\alpha}_m'' + \frac{\gamma_m^{nr}}{\gamma_m} \bar{\alpha}_m'', \quad (42)$$

where the first term represents scattering contribution and satisfies the relation

$$\frac{\gamma_m^r}{\gamma_m} \bar{\alpha}_m'' = \frac{2}{3} \left(\frac{\omega}{c} \right)^3 \bar{\alpha}_m \cdot \bar{\alpha}_m^*. \quad (43)$$

Since $\bar{\alpha}_m$ is proportional to the plasmonic system volume, in nanoplasmonic systems scattering is suppressed so that extinction is dominated by absorption, given by second term in Eq. (42). Near the resonance, the resonance part of plasmon polarizability takes the form

$$\bar{\alpha}_m(\omega) = \frac{\omega_m}{4U_m} \frac{\mathbf{P}_m \mathbf{P}_m}{\omega_m - \omega - i\gamma_m/2}. \quad (44)$$

The approach developed in this section will be used in the rest of this paper to describe spontaneous decay of a QE coupled to plasmonic resonator.

IV. PLASMON LDOS, MODE DENSITY AND MODE VOLUME

We are now in position to derive the plasmon LDOS that accounts for both Ohmic and radiative losses. On length scale well below the diffraction limit, surface plasmons are mostly electronic excitations interacting weakly with the radiation field. In this section we show that, within our approach, the plasmon mode volume can be defined in natural way as the inverse of plasmon mode density, which describes spatial distribution of plasmon states. We derive explicit expression for the plasmon mode volume at hot spot near sharp metal tip which scales with the metal volume while being highly sensitive to distance from the tip.

A. Mode volume for plasmonic systems

The standard expression for electromagnetic LDOS, $\rho(\omega, \mathbf{r}) = (2\omega/\pi c^2) \text{Im} \text{Tr}[\bar{\mathbf{G}}(\omega; \mathbf{r}, \mathbf{r})]$, can be written in

terms of near-field Green dyadic (4) as

$$\rho(\omega, \mathbf{r}) = \frac{1}{2\pi^2\omega} \text{Im} \text{Tr} \bar{\mathbf{D}}(\omega; \mathbf{r}, \mathbf{r}). \quad (45)$$

Near plasmon resonance and with help of the plasmon Green dyadic (20), we obtain the plasmon LDOS as

$$\rho_m(\omega, \mathbf{r}) = \frac{1}{4\pi^2 W_m} \frac{\mathbf{E}_m^2(\mathbf{r})}{1 + 4Q_m^2(\omega/\omega_m - 1)^2}, \quad (46)$$

where plasmon quality factor is given by

$$Q_m = \frac{\omega_m}{\gamma_m} = \frac{\omega_m U_m}{W_m}, \quad (47)$$

and dissipated power $W_m = W_m^{nr} + W_m^r$ incorporates all plasmon damping channels. As function of frequency, the LDOS has Lorentzian shape and, at resonance, is proportional to the plasmon field intensity normalized by mode's dissipated power: $\rho(\omega_m, \mathbf{r}) = \mathbf{E}_m^2(\mathbf{r})/4\pi^2 W_m$.

The plasmon LDOS (46) describes distribution of plasmon states in unit volume and frequency interval. Frequency integration of LDOS yields *plasmon mode density*

$$\rho_m(\mathbf{r}) = \int d\omega \rho_m(\omega, \mathbf{r}) = \frac{\omega_m \mathbf{E}_m^2(\mathbf{r})}{8\pi Q_m W_m} = \frac{\mathbf{E}_m^2(\mathbf{r})}{8\pi U_m}, \quad (48)$$

which describes spatial distribution of plasmon field intensity. Note that, in contrast to LDOS, $\rho(\mathbf{r})$ is normalized by the mode energy, rather than dissipated power, and, hence, is *independent of losses*. With help of Eq. (14), the mode density is explicitly obtained as

$$\rho_m(\mathbf{r}) = \frac{1}{\mathcal{V}_m(\mathbf{r})} = \frac{2\mathbf{E}_m^2(\mathbf{r})}{\int dV \mathbf{E}_m^2(\mathbf{r}) \partial(\omega_m \varepsilon')/\partial \omega_m}, \quad (49)$$

which can be viewed as the inverse *local mode volume* $\mathcal{V}_m(\mathbf{r})$, which characterizes field localization at point \mathbf{r} . The expression (49) is valid for any nanoplasmonic system, including open systems, in contrast to cavity mode volume $\mathcal{V}_{cav} = \int dV \varepsilon(\mathbf{r}) \mathbf{E}_m^2(\mathbf{r}) / [\varepsilon(\mathbf{r}) \mathbf{E}_m^2(\mathbf{r})]$, where QE location \mathbf{r} is presumed to be inside the cavity. Note that the plasmon mode density and mode volume, given by Eq. (49), are real functions of plasmon field intensity.

B. Plasmon mode volume near metallic tip

The largest plasmonic enhancements occur if QE is located at *hot spot* – a small region characterized by very high mode density (or very small mode volume), e.g., near sharp tip of metal nanostructure. With help of Eq. (49), the maximal mode density can be estimated by assuming classical field profile near the metal surface. Due to the Gauss law, the local fields do not significantly change inside small metallic structure, while falling off rapidly outside it, so the highest field intensity is achieved near the metal surface,

$$\rho_m(\mathbf{r}) \approx \frac{2}{\omega_m \partial \varepsilon'(\omega_m)/\partial \omega_m} \frac{\mathbf{E}_L^2(\mathbf{r}) + \mathbf{E}_T^2(\mathbf{r})}{V_{\text{met}} ([\mathbf{E}_L^{in}]^2 + \mathbf{E}_T^2)}, \quad (50)$$

where V_{met} is the metal volume. Here, subscripts n and t stand for longitudinal (normal to the tip) and transverse (tangential to the tip) field components, and superscripts in and out indicate local fields at the interface on metal and dielectric side, respectively. The highest field localization is achieved when E_T , which is continuous across the metal-dielectric interface, is much smaller than E_L . Assuming that the local field is polarized along the tip, i.e., $E_L \gg E_T$, and using boundary condition for normal field component $E_L^{out} = \varepsilon'(\omega_m) E_L^{in}$, we obtain the mode density projected along the tip:

$$\rho_L(\mathbf{r}) = \frac{1}{\mathcal{V}_L(\mathbf{r})} = \frac{1}{V_{\text{met}}} \frac{2|\varepsilon'(\omega_m)|^2 \tilde{E}_L^2(\mathbf{r})}{\omega_m \partial \varepsilon'(\omega_m)/\partial \omega_m}, \quad (51)$$

where $\tilde{E}_L(\mathbf{r}) = E_L(\mathbf{r})/E_L^{out}$ is normal field component at point \mathbf{r} near the tip normalized by its value at the tip. Although mode volume near hot spot scales with metal volume V_{met} , the ratio $V_{\text{met}}/\mathcal{V}_L = V_{\text{met}} \rho_L$ depends on the proximity of QE to the tip. Although the mode density is highest at the tip ($\tilde{E}_L = 1$), it is expected to saturate below distances $\sim v_F/\omega$ as the nonlocal effects become dominant [53]. Note for noble metals, this length scale is below 1 nm in the plasmonic frequency range.

V. PURCELL FACTOR AND ENHANCEMENT FACTOR FOR POWER SPECTRUM

Purcell factor characterizes enhancement of the QE decay rate due to ET between QE and plasmonic resonator. Part of the transferred energy is radiated away by the plasmonic antenna, while the rest is dissipated due to the Ohmic losses in metal. In this section, we derive explicit expressions for Purcell factor for spontaneous decay rate and enhancement factor for radiated power spectrum.

A. QE-plasmon ET rate and Purcell factor

The ET rate between a QE situated at \mathbf{r}_0 with dipole moment $\mathbf{p} = \mu \mathbf{n}$ and resonant plasmon mode is straightforwardly obtained from Eq. (5) with help of the plasmon Green function (20) as

$$\gamma_{et}(\omega) = \frac{\mu^2 Q_m}{\hbar U_m} \frac{[\mathbf{n} \cdot \mathbf{E}_m(\mathbf{r}_0)]^2}{1 + 4Q_m^2(\omega/\omega_m - 1)^2}. \quad (52)$$

As function of QE emission frequency ω , the ET rate has Lorentzian form and reaches its maximum at $\omega = \omega_m$. In terms of projected mode volume on QE dipole direction,

$$\rho_m^n(\mathbf{r}) = \frac{1}{\mathcal{V}_m^n(\mathbf{r})} = \frac{2 [\mathbf{n} \cdot \mathbf{E}_m(\mathbf{r})]^2}{\int dV \mathbf{E}_m^2 \partial(\omega_m \varepsilon')/\partial \omega_m}, \quad (53)$$

the QE-plasmon ET rate takes the form

$$\gamma_{et}(\omega) = \frac{8\pi\mu^2}{\hbar \mathcal{V}_m^n(\mathbf{r}_0)} \frac{Q_m}{1 + 4Q_m^2(\omega/\omega_m - 1)^2}. \quad (54)$$

Normalizing the QE-plasmon ET rate at resonance frequency, $\gamma_{et}(\omega_m) = 8\pi\mu^2Q_m/\hbar\mathcal{V}_m^n$, by the free-space QE spontaneous decay rate (3), we finally obtain the Purcell factor for a QE coupled to resonant plasmon mode,

$$F_p = \frac{6\pi Q_m}{k^3 \mathcal{V}_m^n} = \frac{12\pi Q_m [\mathbf{n} \cdot \mathbf{E}_m(\mathbf{r}_0)]^2}{k^3 \int dV \mathbf{E}_m^2 \partial(\omega_m \varepsilon') / \partial \omega_m}, \quad (55)$$

which extends the cavity Purcell factor (1) to plasmonic resonators. For QE at the hot spot near metallic tip, with help of Eq. (51), we obtain

$$F_p^{\text{tip}} = \frac{12\pi Q_m |\varepsilon'(\omega_m)|^2}{k^3 V_{\text{met}} \omega_m \partial \varepsilon'(\omega_m) / \partial \omega_m} [\mathbf{n} \cdot \tilde{\mathbf{E}}_L(\mathbf{r}_0)]^2, \quad (56)$$

where $\mathbf{n} \cdot \tilde{\mathbf{E}}_L(\mathbf{r}_0)$ stands for projection of normalized field component along the tip onto QE's dipole orientation \mathbf{n} . The Purcell factor is maximal when QE dipole is oriented along the tip, while for transverse dipole orientation there is no significant enhancement.

B. Radiated power spectrum and the enhancement factor

Part of the energy transferred from the QE to resonant plasmon mode is radiated away by the plasmonic antenna, leading to overall enhancement of radiated power observed, e.g., in plasmon-enhanced fluorescence experiments [5–11]. While plasmon's radiative decay rate (27) is typically much larger than that of individual QE, i.e., $\gamma_m^r \gg \gamma_0^r$, significant part of the transferred energy is dissipated in the metal at rate (21), so that the enhancement factor depends on radiation efficiency of the plasmonic antenna $\eta_m = \gamma_m^r / \gamma_m$.

The power radiated by a QE placed at position \mathbf{r}_0 near plasmonic antenna is obtained by integrating Poynting's vector $S = (c/8\pi)|\mathbf{E}(\mathbf{r})|^2$ over remote surface enclosing the system, where $\mathbf{E}(\mathbf{r})$ is the QE electric field [37]

$$\mathbf{E}(\mathbf{r}) = \bar{\mathbf{D}}(\omega; \mathbf{r}, \mathbf{r}_0) \cdot \mathbf{p}, \quad (57)$$

and $\bar{\mathbf{D}}(\omega; \mathbf{r}, \mathbf{r}_0)$ is the Green dyadic (4). In order to extract far field contribution, we use the Dyson equation (35). Replacing the near-field Green dyadic $\bar{\mathbf{D}}$ in the integrand by plasmon Green dyadic (20), the QE-generated far field (57) takes the form

$$\begin{aligned} \mathbf{E}(\mathbf{r}) &= \bar{\mathbf{D}}_0(\omega; \mathbf{r} - \mathbf{r}_0) \cdot \mathbf{p} \\ &+ \frac{\omega_m}{4U_m} \frac{\mathbf{E}_m(\mathbf{r}_0) \cdot \mathbf{p}}{\omega_m - \omega - i\gamma_m/2} \int dV' \bar{\mathbf{D}}_0(\omega; \mathbf{r} - \mathbf{r}') \cdot \mathbf{P}_m(\mathbf{r}'). \end{aligned} \quad (58)$$

Using far field asymptotics of free-space Green function $\bar{\mathbf{D}}_0(\omega; \mathbf{r}) = (\omega/c)^2 (e^{ikr}/r) (\mathbf{I} - \hat{\mathbf{r}}\hat{\mathbf{r}})$, straightforward integration of Poynting's vector over remote spherical surface yields the radiated power

$$W_r(\omega) = \frac{\omega^4}{3c^3} \left| \mathbf{p} + \frac{\omega_m}{4U_m} \frac{\mathbf{P}_m[\mathbf{E}_m(\mathbf{r}_0) \cdot \mathbf{p}]}{\omega_m - \omega - i\gamma_m/2} \right|^2, \quad (59)$$

where the second term represents contribution of the plasmonic antenna with dipole moment \mathbf{P}_m . Near the resonance, the plasmon emission is dominant and, disregarding the first nonresonant term, we obtain

$$W_r(\omega) = \frac{\mu^2 \omega^4}{3c^3} \frac{\gamma_m^r \gamma_{et}(\omega)}{\gamma_m \gamma_0^r}, \quad (60)$$

where QE-plasmon ET rate $\gamma_{et}(\omega)$ is given by Eq. (54), and radiative decay rates γ_0^r and γ_m^r are given by Eqs. (3) and (27), respectively. Normalizing $W_r(\omega)$ by spectral power $W_r^0 = \mu^2 \omega^4 / 3c^3$ radiated by isolated QE [37], we obtain the enhancement factor for power spectrum

$$M(\omega) = \frac{F_p \eta_m}{1 + 4Q_m^2(\omega/\omega_m - 1)^2}, \quad (61)$$

where the Purcell factor F_p is given by Eq. (55) and plasmon radiation efficiency η_m is given by (29). Near the resonance, $|\omega - \omega_m| \ll \gamma_m$, we obtain

$$M(\omega_m) = F_p \eta_m = \frac{6\pi Q_m}{k^3 \mathcal{V}_m^n} \eta_m, \quad (62)$$

which represents general relation between the Purcell factor for spontaneous decay and maximal enhancement factor. For high radiation efficiency $\eta \sim 1$, the enhancement factor is comparable to the Purcell factor, i.e., energy is radiated by the plasmonic antenna at approximately same rate as it is being received from the QE.

Note, however, that the relation (62) overestimates the enhancement factor as it does not account for the ET to dark off-resonant modes which leads to radiation quenching as QE approaches the metal surface. In this case, the fraction of energy transferred from QE to the bright plasmon mode is $q = F_p / \sum_l F_p^{(l)}$, where $F_p^{(l)}$ are Purcell factors for all modes, and, correspondingly, the enhancement factor M is suppressed by quenching factor q .

VI. NUMERICAL RESULTS AND DISCUSSION

To illustrate our theory, we performed numerical calculations for a QE coupled to longitudinal plasmon mode oscillating, with frequency ω_L , along Au nanorod, which is modeled here by prolate spheroid with semi-major and semi-minor axes a and b , respectively (see schematics in Fig. 1). This needle-shaped structure is characterized by relatively high radiation efficiency while, at the same time, possesses hot spots near the tips, where the plasmon field is highly localized. We assume that Au nanorod is submerged into water ($\varepsilon_s = 1.77$) and use experimental Au dielectric function $\varepsilon(\omega) = \varepsilon'(\omega) + i\varepsilon''(\omega)$ in all calculations. The dielectric constant ε_s of surrounding medium is restored in all expressions via replacements: $c \rightarrow c/\varepsilon_s$, $\varepsilon(\omega, \mathbf{r}) \rightarrow \varepsilon(\omega, \mathbf{r})/\varepsilon_s$, and $\mu^2 \rightarrow \mu^2/\varepsilon_s$. Analytical expressions for spheroidal particles are provided in the Appendix along with other technical detail, and here we only discuss the results of numerical calculations.

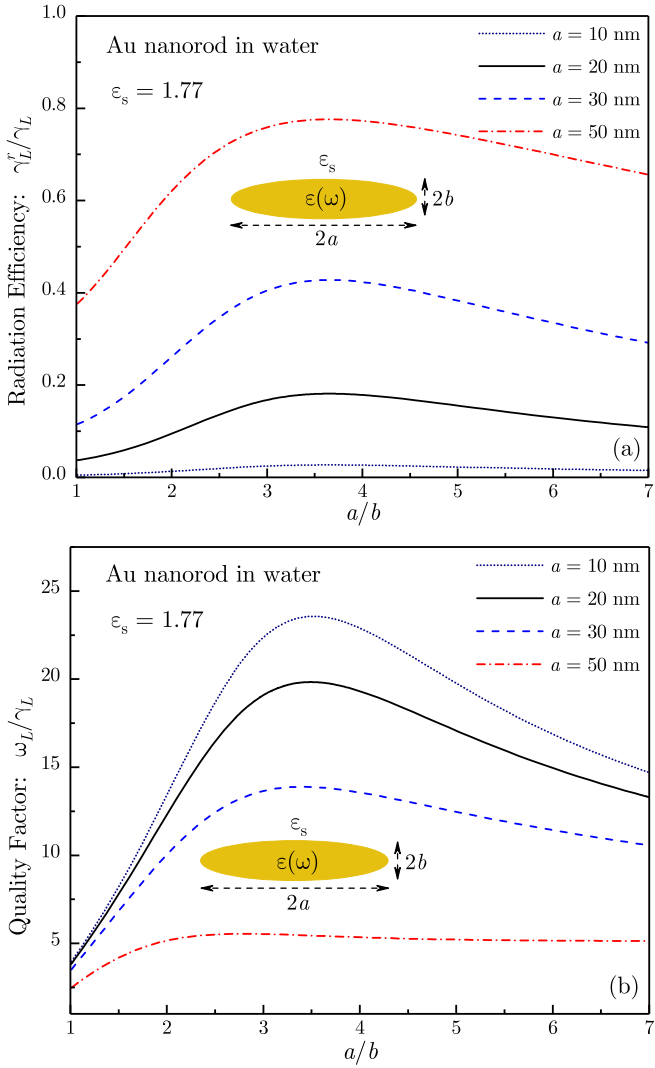


FIG. 1. Plasmon radiation efficiency η_L (a), and quality factor Q_L (b) plotted against aspect ratio a/b for different nanorod sizes. Inset: Schematics of prolate spheroidal particle.

In Fig. 1 we show calculated plasmon radiation efficiency $\eta_L = \gamma_L^r/\gamma_L$ and quality factor $Q_L = \omega_L/\gamma_L$ which include both radiative and Ohmic losses. As expected, the increase of η_L with nanorod overall size [see Fig. 1(a)] is accompanied by reduction of quality factor [see Fig. 1(b)] due to overall increase of the plasmon decay rate $\gamma_L = \gamma_L^r + \gamma_L^{nr}$. The maximal η_L and Q_L are reached for aspect ratio a/b in the range $3 \div 5$, corresponding to plasmon wavelength range $650 \div 800$ nm, where $\epsilon''(\omega)$ for Au reaches its minimum, which translates to lowest Ohmic losses and, hence, highest η_L and Q_L , except for the largest nanorod ($a = 50$ nm), where the plasmon decay is dominated by radiative channel [see Fig. 1(b)].

To study field localization at hot spot, in Fig. 2 we plot plasmon mode density ρ_L projected along nanorod symmetry axis, given by Eq. (51) that is exact for spheroidal shape, and normalized by the metal volume as function of distance d to the nanorod tip for several values of aspect ratio. To account for field enhancement saturation

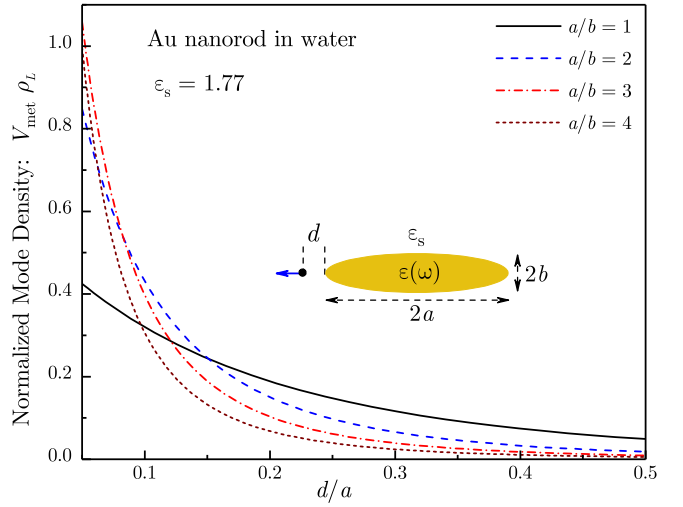


FIG. 2. Normalized mode density (inverse mode volume) projected along Au nanorod is plotted against the distance to nanorod tip for different aspect ratios a/b at fixed a .

due to nonlocal effects [53], we restrict minimal distance to the tip by $d_{\min} = 0.05a$, and change the nanorod volume by reducing b at fixed a . For aspect ratios in the range $2 \div 4$, i.e., when the system has hot spots near the tips, the mode volume $\mathcal{V}_L = 1/\rho_L$ exhibits nearly universal behavior reaching V_{met} in the hot spot region and rapidly decreasing with increasing d .

Consider now spontaneous decay of a QE at distance d from the nanorod tip with its dipole oriented normally to the metal surface (see schematics in Fig. 3). We assume that QE is situated at fixed distance $d = 1$ nm from the tip, where the plasmon field is highly localized. In Fig. 3, we show the QE-plasmon ET rate (54), normalized by free-space decay rate (3), and the enhancement factor for power spectrum (61) plotted against QE emission frequency ω for different a but at fixed aspect ratio $a/b = 3.0$. The amplitude of frequency Lorentzian $\gamma_{et}(\omega)/\gamma_0^r$ in Fig. 3(a) is given by the Purcell factor (55), which, near hot spot, scales as Q_L/k^3V_{met} [see Eq. (56)]. With increasing nanorod size, the Purcell factor sharply decreases due to combined effect of decreasing Q_L and, more importantly, increasing k^3V_{met} . However, the enhancement factor $M(\omega)$ in Fig. 3(b) exhibits more complicated behavior: its amplitude $F_p\eta_L$ first sharply increases, as a changes from 10 nm to 20 nm, due to rapid change of η_L and then, for larger a , falls down as the metal volume effect in F_p takes over.

In Fig. 4, we show Purcell factor F_p and enhancement factor at resonance frequency $M(\omega_L) = F_p\eta_L$ plotted against the distance d to the nanorod tip for several overall sizes. With QE moving away from the tip, both F_p and $M(\omega_L)$ decrease by up to two orders of magnitude as d increases to $a/2$, indicating that the plasmon field is highly localized near the tips (see Fig. 2). Note that since, in Fig. 4, the distance is measured in units of nanorod size, the same starting point $d = 0.05a$ for each curve translates into different initial distance to the metal

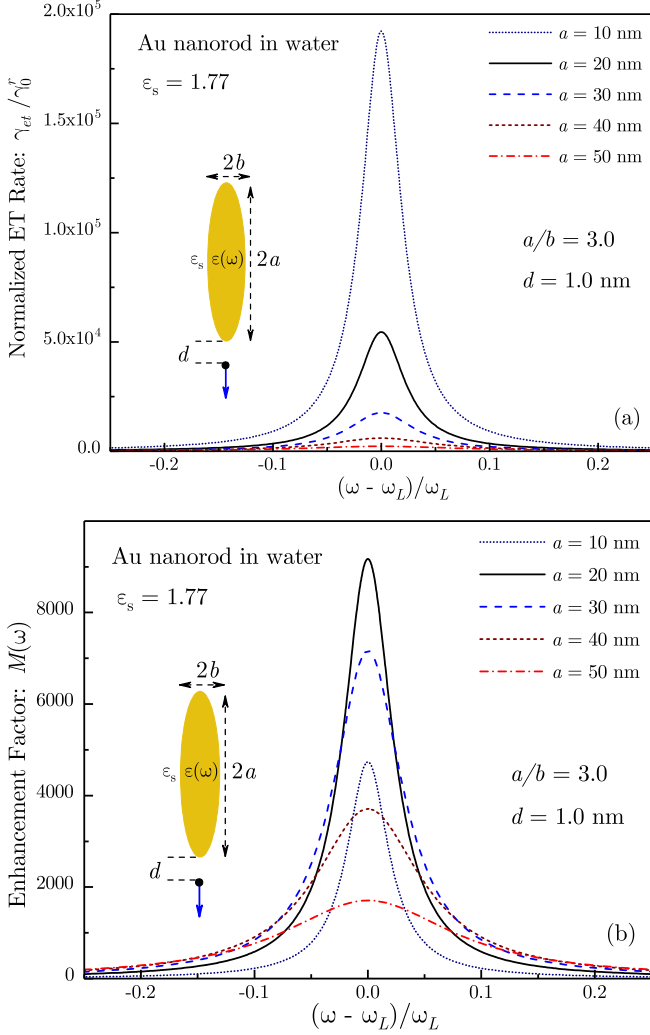


FIG. 3. Frequency dependence of normalized QE-plasmon ET rate and enhancement factor for power spectrum for normally-oriented QE at distance 1.0 nm from Au nanorod tip is plotted for different nanorod sizes and fixed aspect ratio $a/b = 3.0$.

surface. After rescaling is made to bring initial distances to the same numerical value (e.g., 1.0 nm), the order of curves in Fig. 4 follows that in Fig. 3. Overall, Figs. 3 and 4 indicate that the Purcell factor and enhancement factor are highly sensitive to the system size due to scaling of plasmon mode volume with metal volume (see Fig. 2) and, to lesser degree, size-dependence of plasmon quality factor and radiation efficiency (see Fig. 1).

VII. CONCLUSIONS

In summary, here we presented a theory for spontaneous decay of a quantum emitter coupled to localized plasmon mode in metal-dielectric structure characterized by dispersive dielectric function which incorporates. For plasmonic systems with characteristic size below the diffraction limit, we derived explicit expressions for plasmon radiative decay rate, which determines radiation ef-

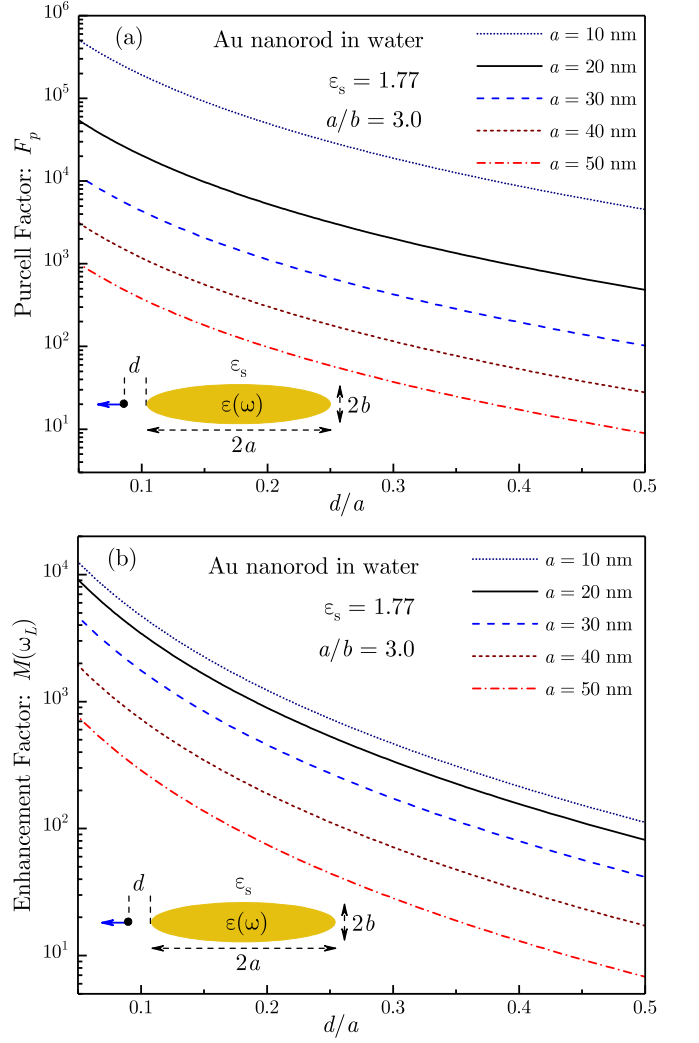


FIG. 4. Distance dependence of Purcell factor and enhancement factor for power spectrum at resonance frequency is plotted for normally-oriented QE near Au nanorods of different sizes and fixed aspect ratio a/b .

ficiency of plasmonic antenna, and optical polarisability, which defines the system response to external field. Using these results, we extended our approach [49] to derive plasmon Green function that now includes plasmon interaction with radiation field, and obtained explicit expressions for the plasmon local density of states and mode volume. We estimated the plasmon mode volume at hot spot near sharp tip of metal nanostructure and demonstrated that it scales with the metal volume, although its actual value is highly sensitive to QE's separation from the tip. Using our approach, we recovered the usual form of Purcell factor, but now for plasmonic resonators, and established its relation with the enhancement factor for radiated power. Finally, we illustrated our approach by presenting numerical results for QE situated near the tip of Au nanorod.

This work was supported in part by NSF grants No. DMR-1610427 and No. HRD-1547754.

Appendix A: Potentials and fields in spheroidal particles

Consider a prolate spheroid with semiaxis a along the symmetry axis and semiaxis b in the symmetry plane ($a > b$). We use standard notations for spheroidal coordinates (ξ, η, ϕ) where ξ is "radial" coordinate while $\eta = \cos\theta$ and ϕ parametrise the surface. The scaling factors are given by

$$h_\xi = f \sqrt{\frac{\xi^2 - \eta^2}{\xi^2 - 1}}, \quad h_\eta = f \sqrt{\frac{\xi^2 - \eta^2}{1 - \eta^2}}, \\ h_\phi = f \sqrt{(\xi^2 - 1)(1 - \eta^2)}, \quad (\text{A1})$$

where $f = \sqrt{a^2 - b^2}$ is half distance between the foci, and spheroid surface corresponds to $\xi_1 = a/f$. The volume and surface elements are, respectively, $dV = h_\xi h_\eta h_\phi d\xi d\eta d\phi$ and $dS = h_\eta h_\phi d\eta d\phi$, and the gradient operator is $\nabla = \hat{\xi} h_\xi^{-1} \partial/\partial\xi + \hat{\eta} h_\eta^{-1} \partial/\partial\eta + \hat{\phi} h_\phi^{-1} \partial/\partial\phi$.

The potentials for longitudinal and transverse dipole modes are

$$\Phi_L = f R_L(\xi) P_1(\eta), \quad \Phi_T = f R_T(\xi) P_1^1(\eta) \cos\phi. \quad (\text{A2})$$

For a metallic spheroid with permittivity $\varepsilon(\omega)$ in a medium with dielectric constant ε_s , the radial components for longitudinal mode are

$$R_L(\xi) = P_1(\xi), \quad \text{for } \xi < \xi_1, \\ R_L(\xi) = Q_1(\xi) P_1(\xi_1)/Q_1(\xi_1), \quad \text{for } \xi > \xi_1. \quad (\text{A3})$$

The plasmon frequencies ω_L follow from the continuity of $\varepsilon R'(\xi)$ across the metal/dielectric interface.

Appendix B: Plasmon energy in spheroidal particle

In the quasistatic approximation, the plasmon mode energy comes solely from the metal volume and has the form

$$U_m = \frac{\omega_m}{16\pi} \frac{\partial \varepsilon(\omega_m)}{\partial \omega_m} \int dV_{\text{met}} |\mathbf{E}_m|^2 \\ = \frac{\omega_m}{16\pi} \frac{\partial \varepsilon(\omega_m)}{\partial \omega_m} \int dS \Phi \nabla_n \Phi, \quad (\text{B1})$$

where V_{met} and S are volume and surface of metal nanoparticle, respectively, and ∇_n is the normal derivative. Using Eqs. (A3), we obtain

$$U_m = V_{\text{met}} \frac{\omega_m}{16\pi} \frac{\partial \varepsilon(\omega_m)}{\partial \omega_m} = ab^2 \frac{\omega_m}{12} \frac{\partial \varepsilon(\omega_m)}{\partial \omega_m}. \quad (\text{B2})$$

Note that the energy difference between longitudinal and transverse modes comes solely from different ω_m .

Appendix C: Plasmon radiative decay in spheroidal particle

The decay rate of a plasmon mode in metal-dielectric system embedded in dielectric medium ε_s has the form

$$\gamma_m^r = \frac{n_s \omega_m^4}{3c^3} \frac{|\mathbf{P}_m|^2}{U_m} \quad (\text{C1})$$

where $\mathbf{P}_m = (4\pi)^{-1} \int dV \mathbf{E}_m(\mathbf{r}) [\varepsilon'(\omega_m, \mathbf{r}) - \varepsilon_s]$ is plasmon dipole moment. Due to Gauss law, \mathbf{P}_m can be written as surface integral

$$\mathbf{P}_m = \frac{\varepsilon'(\omega_m) - \varepsilon_s}{4\pi} \int dS \Phi_m(\mathbf{s}) \mathbf{n}. \quad (\text{C2})$$

For spheroidal particles, the potentials are given by (A2) and the normal vectors are $\mathbf{n} = \hat{\xi}$. Using addition formula $\hat{\xi} \cdot \hat{\xi}' = \cos\theta \cos\theta' + \sin\theta \sin\theta' \cos(\phi - \phi')$ for spheroidal coordinates ($\eta = \cos\theta$), we obtain

$$|\mathbf{P}_L|^2 = \left[\frac{a^2 b}{3} [\varepsilon'(\omega_m) - \varepsilon_s] g_L(\xi_1) \right]^2, \quad (\text{C3})$$

with $\xi_1 = a/\sqrt{a^2 - b^2}$. Here, function $g_L(\xi)$ is given by

$$g_L(\xi) = \frac{3\xi^3}{8} \arctan \frac{1}{\sqrt{\xi^2 - 1}} - \frac{3(\xi^2 - 2)}{8\xi} \sqrt{\xi^2 - 1}, \quad (\text{C4})$$

and it changes in the range 0.5-1.0, reaching the upper limit in the sphere case ($\xi \rightarrow \infty$). Using Eqs. (C3) and (B2), the plasmon radiative decay rate can be evaluated:

$$\gamma_L^r = \frac{4n_s \omega_m^3 a^3}{9c^3} \frac{[\varepsilon'(\omega_m) - \varepsilon_d]^2}{\partial \varepsilon'(\omega_m) / \partial \omega_m} g_L^2(\xi_1), \quad (\text{C5})$$

Note that radiative rate for spheroidal particle scales as a^3 rather than as particle volume, implying high radiation efficiency for low-metal-volume elongated particles. For spherical particle ($a = b$), we have $g_L = 1$ and $\varepsilon'(\omega_m) = -2\varepsilon_d$ at resonance, thus recovering the plasmon radiative decay rate for nanosphere.

Appendix D: Mode volume and Purcell factor for spheroidal particles

Using the Gauss law and expressing local fields in terms of potentials, the mode density projected along nanorod major axis takes the form

$$\rho_L(\mathbf{r}) = \frac{2}{\omega_m \partial \varepsilon'(\omega_m) / \partial \omega_m} \frac{|\nabla_n \Phi_m(\mathbf{r})|^2}{\int dS_1 \Phi_m^* \nabla_n \Phi_m}, \quad (\text{D1})$$

where integration takes place over the metal surface. For \mathbf{r} at the distance d from the tip of a prolate spheroidal

particle with major and minor semiaxes a and b , respectively, so that $\xi_1 = a/\sqrt{a^2 - b^2}$ at the surface, and using that $h_\xi = f$ along the z -axis, we obtain

$$\rho_L = \frac{1}{V_L} = \frac{2}{V_{\text{met}} \omega_L} \left[\frac{\partial \varepsilon'(\omega_L)}{\partial \omega_L} \right]^{-1} \left[\frac{Q'_1(\xi) \xi_1}{Q_1(\xi_1)} \right]^2, \quad (\text{D2})$$

where $\xi = (a+d)/f$, $V_{\text{met}} = 4\pi ab^2/3$ is Au nanorod volume, and plasmon frequency ω_L follows from boundary condition $\varepsilon'(\omega_L) = \varepsilon_s Q'_1(\xi_1) \xi_1 / Q_1(\xi_1)$. In the limit of spherical particle of radius a , i.e., $f \rightarrow 0$ and $\xi \rightarrow \infty$ as

$b \rightarrow a$, we have $Q(\xi) \approx 1/3\xi^2$, yielding

$$\rho_{\text{sph}} = \frac{1}{V_{\text{sph}}} = \frac{6}{\pi \omega_L} \left[\frac{\partial \varepsilon'(\omega_L)}{\partial \omega_L} \right]^{-1} \frac{a^3}{(a+d)^6}. \quad (\text{D3})$$

Note that for random dipole orientations, the orientational averaging results in the additional factor $1/3$ in Eqs. (D2) and (D3). Finally, the Purcell factor for QE at distance d from the nanorod tip is given by

$$F_p = \frac{12\pi \varepsilon_s Q_L}{k^3 V_{\text{met}} \omega_L \partial \varepsilon'(\omega_L) / \partial \omega_L} \left[\frac{Q'_1(\xi) \xi_1}{Q_1(\xi_1)} \right]^2, \quad (\text{D4})$$

and scales as $(k^3 V_{\text{met}})^{-1}$.

[1] S. A. Maier and H. A. Atwater, *J. Appl. Phys.* **98**, 011101 (2005).
[2] E. Ozbay, *Science* **311**, 189 (2006).
[3] M. I. Stockman, in *Plasmonics: Theory and Applications*, edited by T. V. Shahbazyan and M. I. Stockman (Springer, New York, 2013).
[4] E. C. Le Ru and P. G. Etchegoin, *Principles of Surface-Enhanced Raman Spectroscopy* (Elsevier, 2009).
[5] E. Dulkeith, A. C. Morteani, T. Niedereichholz, T. A. Klar, J. Feldmann, S. A. Levi, F. C. J. M. van Veggel, D. N. Reinhoudt, M. Moller, and D. I. Gittins, *Phys. Rev. Lett.* **89**, 203002 (2002).
[6] O. Kulakovitch, N. Strekal, A. Yaroshevich, S. Maskevich, S. Gaponenko, I. Nabiev, U. Woggon, and M. Artemyev, *Nano Lett.* **2**, 1449 (2002).
[7] P. Anger, P. Bharadwaj, and L. Novotny, *Phys. Rev. Lett.* **96**, 113002 (2006).
[8] S. Kühn, U. Hakanson, L. Rogobete, and V. Sandoghdar, *Phys. Rev. Lett.* **97**, 017402 (2006).
[9] F. Tam, G. P. Goodrich, B. R. Johnson, and N. J. Halas, *Nano Lett.* **7**, 496 (2007).
[10] R. Bardhan, N. K. Grady, J. R. Cole, A. Joshi, and N. J. Halas, *ACS Nano* **3**, 744 (2009).
[11] T. Ming, L. Zhao, Z. Yang, H. Chen, L. Sun, J. Wang, and C. Yan, *Nano Lett.* **9**, 3896 (2009).
[12] J. Bellessa, C. Bonnand, J. C. Plenet, and J. Mugnier, *Phys. Rev. Lett.* **93**, 036404 (2004).
[13] Y. Sugawara, T. A. Kelf, J. J. Baumberg, M. E. Abdelsalam, and P. N. Bartlett, *Phys. Rev. Lett.* **97**, 266808 (2006).
[14] G. A. Wurtz, P. R. Evans, W. Hendren, R. Atkinson, W. Dickson, R. J. Pollard, A. V. Zayats, W. Harrison, and C. Bower, *Nano Lett.* **7**, 1297 (2007).
[15] N. T. Fofang, T.-H. Park, O. Neumann, N. A. Mirin, P. Nordlander, and N. J. Halas, *Nano Lett.* **8**, 3481 (2008).
[16] T. K. Hakala, J. J. Toppari, A. Kuzyk, M. Pettersson, H. Tikkanen, H. Kunttu, and P. Torma, *Phys. Rev. Lett.* **103**, 053602 (2009).
[17] D. E. Gomez, K. C. Vernon, P. Mulvaney, and T. J. Davis, *Nano Lett.* **10**, 274 (2010).
[18] A. Manjavacas, F. J. Garcia de Abajo, and P. Nordlander, *Nano Lett.* **11**, 2318 (2011).
[19] A. Berrier, R. Cools, C. Arnold, P. Oermans, M. Crego-Calama, S. H. Brongersma, and J. Gomez-Rivas, *ACS Nano* **5**, 6226 (2011).
[20] A. Salomon, R. J. Gordon, Y. Prior, T. Seideman, and M. Sukharev, *Phys. Rev. Lett.* **109**, 073002 (2012).
[21] S. Aberra Guebrou, C. Symonds, E. Homeyer, J. C. Plenet, Y. N. Gartstein, V. M. Agranovich, and J. Bellessa, *Phys. Rev. Lett.* **108**, 066401 (2012).
[22] T. Antosiewicz, S. P. Apell, and T. Shegai, *ACS Photonics*, **1**, 454 (2014).
[23] A. De Luca, R. Dham, A. R. Rashed, C. Coutant, S. Ravaine, P. Barois, M. Infusino, and G. Strangi, *Appl. Phys. Lett.* **104**, 103103 (2014).
[24] D. J. Bergman and M. I. Stockman, *Phys. Rev. Lett.*, **90**, 027402, (2003).
[25] M. I. Stockman, *Nature Photon.* **2**, 327, (2008).
[26] M. A. Noginov, G. Zhu, A. M. Belgrave, R. Bakker, V. M. Shalaev, E. E. Narimanov, S. Stout, E. Herz, T. Suteewong and U. Wiesner, *Nature*, **460**, 1110, (2009).
[27] R. Carminati, J. J. Greffet, C. Henkel, J. M. Vigoureux, *Opt. Commun.* **261** 368 (2006).
[28] J.-J. Greffet, M. Laroche, and F. Marquier, *Phys. Rev. Lett.* **105**, 117701 (2010).
[29] C. Sauvan, J. P. Hugonin, I. S. Maksymov, and P. Lalanne, *Phys. Rev. Lett.* **110**, 237401 (2013).
[30] R.-C. Ge, P. T. Kristensen, J. F. Young, and S. Hughes, *New J. Phys.* **16**, 113048 (2014).
[31] X. Zambrana-Puyalto, and N. Bonod, *Phys. Rev. B* **91**, 195422 (2015).
[32] A. E. Krasnok, A. P. Slobozhanyuk, C. R. Simovski, S. A. Tretyakov, A. N. Poddubny, A. E. Miroshnichenko, Y. S. Kivshar, and P. A. Belov, *Sci. Rep.* **5**, 12956 (2015).
[33] G. C. des Francs, J Barthes, A Bouhelier, J C Weeber, A Dereux, A Cuche, and C Girard, *J. Opt.* **18** 094005 (2016).
[34] F. Marquier, C. Sauvan, and J.-J. Greffet, *ACS Phot.* **4**, 20912101 (2017).
[35] A. F. Koenderink, *ACS Phot.* **4**, 710-722 (2017).
[36] W. Yan, R. Faggiani, and P. Lalanne, *Phys. Rev. B* **97**, 205422 (2018).
[37] L. Novotny and B. Hecht, *Principles of Nano-Optics* (CUP, New York, 2012).
[38] E. M. Purcell, *Phys. Rev.* **69** (1946) 681.
[39] S. Maier, *Opt. Express* **14**, 1957 (2006).
[40] A. F. Koenderink, *Opt. Lett.* **35** 4208 (2010).

- [41] F. Alpeggiani, S. D'Agostino, and L. C. Andreani, Phys. Rev. B **86**, 035421 (2012).
- [42] P. T. Kristensen, C. Van Vlack, and S. Hughes, Opt. Lett. **37**, 1649 (2012).
- [43] P. T. Kristensen and S. Hughes, ACS Phot. **1**, 2 (2014).
- [44] E. A. Muljarov and W. Langbein, Phys. Rev. B **94**, 235438 (2016).
- [45] C. Sauvan, J. P. Hugonin, R. Carminati, and P. Lalanne, Phys. Rev. A **89**, 043825 (2014).
- [46] P. T. Kristensen, R.-C. Ge, and S. Hughes, Phys. Rev. A **92**, 053810 (2015).
- [47] P. Y. Chen, D. J. Bergman, Y. Sivan, arXiv:1711.00335.
- [48] P. Lalanne, W. Yan, K. Vynck, C. Sauvan, and J.P. Hugonin, Laser Photon. Rev. **12**, 1700113 (2018).
- [49] T. V. Shahbazyan, Phys. Rev. Lett. **117**, 207401 (2016).
- [50] L. D. Landau and E. M. Lifshitz, *Electrodynamics of Continuous Media* (Elsevier, Amsterdam, 2004).
- [51] W. Vogel and D.G. Welsch, *Quantum Optics* (Wiley, 2016).
- [52] T. V. Shahbazyan, Phys. Rev. B **94**, 235431 (2016).
- [53] N. A. Mortensen, S. Raza, M. Wubs, T. Søndergaard, and S. I. Bozhevolnyi, Nat. Commun. **5**, 3809 (2014).